Beneficial Effects of Nitrogen Atomization on an Austenitic Stainless Steel

G.M. JANOWSKI, F.S. BIANCANIELLO, and S.D. RIDDER

Fully dense nitrogenated austenitic stainless steels were produced by gas atomization and HIP consolidation. The base alloy, 304L, contained about 0.15 wt pct nitrogen when melted under a nitrogen atmosphere, and a modified version of 304L with 23 wt pct Cr contained 0.21 wt pct nitrogen. A series of experiments using various combinations of N_2 and Ar as the melt chamber backfill gas and atomizing gas demonstrated that the nitrogen content of the powder was largely controlled by the backfill gas and that the fraction of hollow particles was determined by the atomization gas. The hollow powder particles, which are common in inert-gas atomized materials, were virtually eliminated in the nitrogen atomized powders. Additional atomizing experiments using copper and a nickel-base superalloy indicate that low gas solubility in the metal leads to gas entrapment. Hardness and compression behavior (yield strength and flow stress) are substantially improved with the addition of nitrogen. The results of this study suggest that the properties of nitrogenated stainless steels fabricated in this manner are comparable to other high nitrogen austenitic alloys.

I. INTRODUCTION

ADDITIONS of nitrogen have been shown to enhance the strength, corrosion resistance, and hardness of austenitic stainless steels without sacrificing low-temperature ductility and toughness (*e.g.*, References 1 and 2). An additional advantage of nitrogenated stainless steels is that the precipitation of nitrides along grain boundaries occurs at a slower rate than does the formation of carbides.[1] Therefore, nitrogen-containing stainless steels are less prone to sensitization and more suitable for high-temperature exposure. These qualities make nitrogenated stainless steels candidate materials for applications where moderately high strength, good corrosion resistance, good oxidation resistance, and high toughness are required of nonmagnetic alloys.

One of the limiting factors in the application of nitrogenated stainless steels is the difficulty of incorporating a controllable, homogeneous concentration of nitrogen into the metal. Methods have included melting and casting under high pressure gaseous nitrogen[3,4] or adding nitrogenous materials to the slag during electroslag remelting.[5] A processing route which has not been previously explored is entraining nitrogen during gas atomization followed by forming and/or consolidating the resulting powder by methods such as hot isostatic pressing (HIPping), conventional sintering, or injection molding. By using this fabrication approach, the near-net-shape capabilities of powder metallurgy and the microstructural refinement of rapid solidification can be combined with the improved properties of nitrogenated austenitic stainless steels.

The present article reports on initial results of fabricating a high nitrogen austenitic stainless steel by consolidating powders which were melted under and/or atomized with nitrogen gas. It will be shown that nitrogen is dissolved in the molten metal and retained in the powders during atomization using the NIST supersonic inert gas metal atomizer (SIGMA). In addition, the roles of backfill and atomizing gas in hollow particle formation were examined. Hardness, yield strength, and microstructural data will be presented to demonstrate the viability of this process for manufacturing nitrogenated stainless steels.

II. EXPERIMENTAL PROCEDURE

The 304L rods that were used for melt stock were supplied by Carpenter Technology Corporation (Reading, PA); the composition as given by the supplier is contained in Table I. A modified alloy with 23 wt pct Cr was prepared by adding high purity Cr to the 304L melt stock. This alloy was produced in order to enhance the amount of nitrogen retained in the stainless steel powder. This material will be henceforth referred to as "304L + Cr," and its composition is also shown in Table I. All materials were melted and contained using zirconia crucibles and alumina stopper rods.

The design and operation of NIST's SIGMA have been described elsewhere.[6,7] However, several features of SIGMA are particularly important to these experiments and will be highlighted presently. First, the metal is induction heated to 50 °C above the liquidus temperature (1480 °C) at an absolute pressure of 4 Pa (3×10^{-2} torr). The chamber is then backfilled with either Ar or N_2 gas to 100 kPa (1 atm) and heated to 270 °C of superheat (1700 °C). Since the melt chamber and the atomizing chamber are isolated from each other, it is possible to backfill and atomize using different gases. The induction melting leads to strong liquid mixing which, in turn, results in the molten metal having maximum exposure to the backfill gas. The liquid metal flow is initiated by pulling the alumina stopper rod and disrupted into droplets by close-coupled supersonic gas jets. This atomizer

G.M. JANOWSKI, formerly NRC/NIST Postdoctoral Research Associate, National Institute of Standards and Technology, is Assistant Professor, Department of Materials Science and Engineering, The University of Alabama at Birmingham. Birmingham, AL 35294-4461. F.S. BIANCANIELLO and S.D. RIDDER, Metallurgists, are with the Metallurgy Division, MSEL, National Institute of Standards and Technology, Gaithersburg, MD 20899.

Manuscript submitted January 10, 1992.

Table I. Composition of Base Alloys (Weight Percentages)

Element	304L	304L + Cr
C	0.010	0.009
Mn	1.26	1.19
Si	0.43	0.41
P	0.027	0.026
S	0.001	0.001
Cu	0.41	0.39
Ni	9.89	9.35
Mo	0.69	0.65
Cr	18.55	23.03
Fe	Balance	Balance

design typically produces austenitic stainless steel powders with median particle diameters of approximately 35 μm or finer.

Five atomizing runs were made for the present study. A baseline material, typical of commercial inert gas-atomized 304L powder, was made with argon as both the backfill and atomizing gases. The other three combinations of Ar and N_2 as backfill and atomizing gases were also used to produce powders from the conventional 304L stainless steel. The final powder type was prepared with the 304L + Cr alloy using N_2 as both the backfill and atomizing gas. The melting and atomizing conditions were kept as constant as possible for all five atomizing runs. The designations of the powders and resulting consolidated specimens will be the alloy followed by the backfill gas and the atomizing gas. For example, 304L N_2/Ar is unmodified 304L melted under N_2 and atomized with Ar.

The powder from each atomizing run was initially sieved to −100 mesh (less than 149 μm); this size fraction was approximately 98 pct of the metal that was melted. Representative samples for particle size analysis were obtained by spin riffling the sieved powder. The particle size distributions were determined by sonic sifting the powder into 14 size classes (*e.g.*, −149 + 125 μm, −125 + 105 μm, *etc.*). The particle size distributions are plotted such that the data points are placed in the middle of the size cut. For example, the −125 + 105 μm datum was placed at 115 μm.

The −100 mesh fraction of the as-atomized powders and the as-HIPped specimens were examined using optical metallography. The fraction of porous powder particles was determined quantitatively by manually counting the number of porous particles and total number of particles in representative optical micrographs. Due to sectioning effects, this method underestimates the fraction of powder particles that are hollow but does provide an accurate relative ranking. Between 1500 and 2000 particles from each powder lot were examined.

Consolidated specimens from the five atomizing runs were made by HIPping the −100 mesh powder fractions (a general cut). The powders were evacuated in a high vacuum chamber and sealed in decarburized mild steel cans by electron beam welding. Mild steel was selected as the can material since it is soft and does not react significantly with stainless steel or nitrogen (which minimizes nitrogen loss) at the processing temperatures and times that were employed. The specimens were then hipped at 1200 °C and 150 MPa for 1 hour. No attempt was made to optimize the HIP time and temperature in order to minimize microstructural coarsening or other undesirable effects of thermal exposure. Fully dense specimens were produced from all five powders with this HIPping schedule. The total nitrogen content of the consolidated specimens was determined by the Bureau of Mines, Albany Research Center, Albany, OR, using a commercial oxygen/nitrogen analyzer, which uses inert gas fusion and measures the nitrogen content by thermal conductivity.

The Rockwell A-scale hardness (HRA) of the stainless steels was determined on the as-HIPped specimens. Four to six readings were taken and their values averaged; the difference between the high and low readings was less than one HRA point. This scale was selected (rather than the usual B-scale), since it gives valid results over a much broader range of hardness.

Compression specimens were cut from the hipped material and ground into rectangular parallelepipeds with a 2:1 aspect ratio. The initial strain rate for the testing was 10^{-3}/s. The 0.2 pct offset yield strength and 5 pct flow stress were determined from the load *vs* crosshead position charts. Four to five measurements were made for each sample type; the standard deviations of the yield strengths for each specimen type ranged from 5.4 to 15.9 MPa. Hardness and compression testing was also performed on annealed cast-and-wrought 304L stock as baseline data for a material with no nitrogen. The time and temperature of the annealing treatment that was given to the cast-and-wrought 304L were identical to the powder HIPping conditions.

III. RESULTS

The particle size distributions for the five stainless steel atomizing runs are shown in Figure 1. Cumulative weight percent finer data are given in Figure 1(a), and the weight percent in each size class is given in Figure 1(b). The particle size distributions, although multimodal[8] in characteristic (*i.e.*, there are three peaks in the frequency *vs* particle size plots), were relatively fine with 90 wt pct of the powder less than 100 μm and 50 wt pct less than 35 μm. The dominant particle size (average value of 16 wt pct of total powder) was between 37 and 45 μm, with smaller peaks between 20 and 25 μm (12 wt pct) and between 63 and 74 μm (8 wt pct). There were no significant, systematic differences in the particle size distributions as a function of backfill gas, atomizing gas, or alloy composition.

Optical micrographs of the five as-atomized powders are shown in Figure 2. A significant fraction of the Ar-atomized powders contain pores, while the N_2-atomized powders have very few pores. Quantitative data on the fraction of powder particles that contained pores is shown in Figure 3. Due to the large number of powder particles examined, the observed differences in the fraction of hollow powder particles are statistically significant (95 pct confidence interval), except for the 304L Ar/N_2 and the 304L N_2/N_2 data. The major factor in determining the fraction of hollow particles is the atomizing gas. In

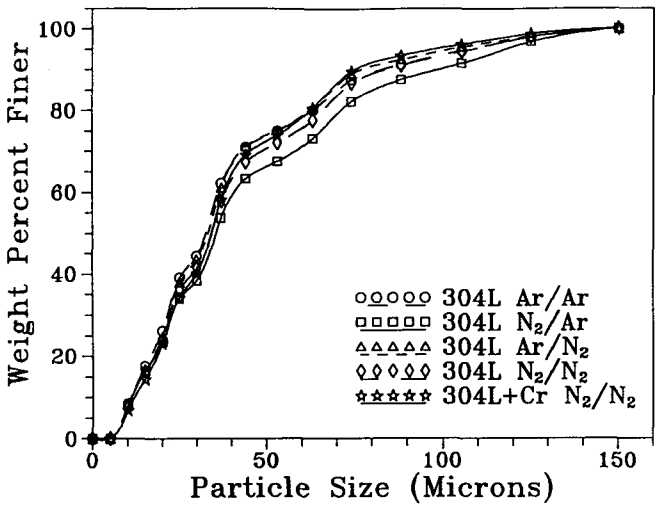

(*a*)

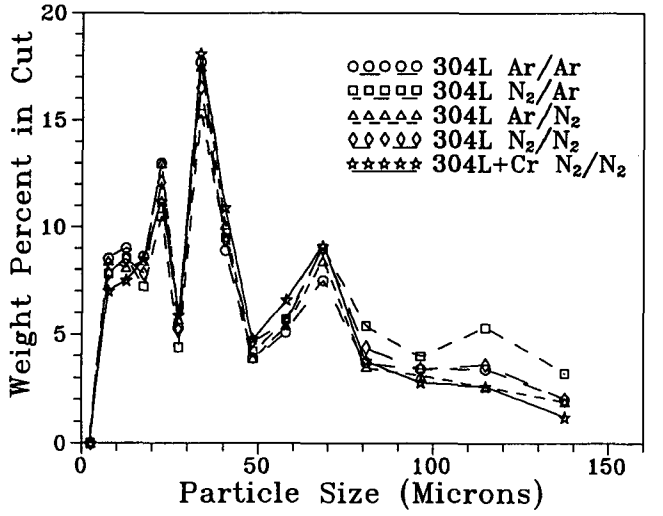

(*b*)

Fig. 1—Particle size distribution curves for 304L with the four permutations of N_2 and Ar as the backfill and atomizing gas. The data for 304L + Cr N_2/N_2 are also shown. The cumulative weight percent finer data is given in (*a*), and the weight percent in each size class is given in (*b*).

addition, the backfill gas type also affects powder porosity; the nitrogen backfilled powders containing fewer hollow particles than Ar backfilled powders atomized with the same gas. The 304L + Cr N_2/N_2 powders had approximately 5 times the number of hollow particles as did the 304L N_2/N_2 powder but about one-sixth the number of porous particles as did the 304L Ar/Ar powders. It should also be noted that the pores are concentrated in the larger sized powder particles, as has been reported previously in other gas atomized powders.[9,10,11]

Micrographs showing the microstructures of 304L Ar/Ar, 304L N_2/N_2, and 304L + Cr N_2/N_2 after HIPping consolidation are contained in Figures 4 and 5. The materials contain few inclusions and pores larger than 1 μm, as can be seen in the as-polished optical micrographs; annealing twins and grain boundaries are evident after etching. The five austenitic stainless steel types are indistinguishable after HIPping at the characterization level of optical microscopy. The densities of the as-HIPped materials were greater than 99.5 pct of the theoretical value, as measured by water immersion.

The nitrogen content of the five austenitic stainless steels is given in Table II. Three generalizations can be made from these data. First, the backfill gas has the strongest effect on the nitrogen content, since the two unmodified 304L trials that were melted under nitrogen had the highest (and nearly identical) nitrogen levels. Second, the atomizing gas has a small role in controlling the nitrogen concentration of 304L. This conclusion is supported by lower nitrogen levels in the Ar-melted samples (compared to N_2-melted) and the similar nitrogen concentrations of specimens melted under the same gas. Finally, alloy composition has a strong effect on the retained nitrogen content, with higher Cr levels being beneficial. The last generalization strongly suggests that the nitrogen levels of N_2-melted, N_2-atomized stainless steels can be enhanced by further modifying the basic 304L composition, as has been previously shown in nitrogenated stainless steels processed using other methods.[3,12]

The Rockwell A-scale hardness, yield strength, and 5 pct flow stress of the nitrogenated stainless steels are plotted in Figures 6 and 7 as a function of nitrogen content. The data for the annealed cast-and-wrought 304L are included in these figures for comparison. The least-squares linear fits for the powder metallurgy alloy data are as follows:

$$\sigma_y^{0.2\ \text{pct}}\ (\text{MPa}) = 214.2 + 1016 \times (\text{wt pct N}) \quad [1]$$

$$\sigma_{\text{flow}}^{5\ \text{pct}}\ (\text{MPa}) = 411.7 + 1220 \times (\text{wt pct N}) \quad [2]$$

$$\text{Hardness (HRA)} = 45.8 + 54.0 \times (\text{wt pct N}) \quad [3]$$

The difference in the best-fit slopes of the yield and 5 pct flow stress plots is statistically significant, since their 95 pct confidence intervals (1016 ± 86 and 1220 ± 79 MPa/wt pct N, respectively) do not overlap.

The addition of nitrogen significantly enhances the yield strength, 5 pct flow stress, and hardness of 304L stainless steel, since atomic nitrogen (not N_2 gas) occupies interstitial lattice sites, similar to carbon in plain carbon steels. The work-hardening rate is also increased, since the slope of the 5 pct flow stress line is greater than that of the 0.2 pct offset yield line. The mechanical property results of this study showing the potent strengthening effects of nitrogen in stainless steels are in general agreement with findings of studies using materials produced by other means, which are compiled in Reference 2. These data also suggest that the principle strengthening effect in the 304L + Cr alloy is the greater nitrogen retention rather than the higher Cr level. This conclusion is based on data from both the 304L and 304L + Cr being plotted on a single line as a function of nitrogen content, which may also be fortuitous.

IV. DISCUSSION

A. *Atomization Behavior/Hollow Powder Particles*

The similarities in the particle size distributions of the five powder types (Figure 1) indicate that the effects of (1) gas type on atomizing parameters (such as viscosity, thermal conductivity, *etc.*) using Ar and N_2 and (2) gas

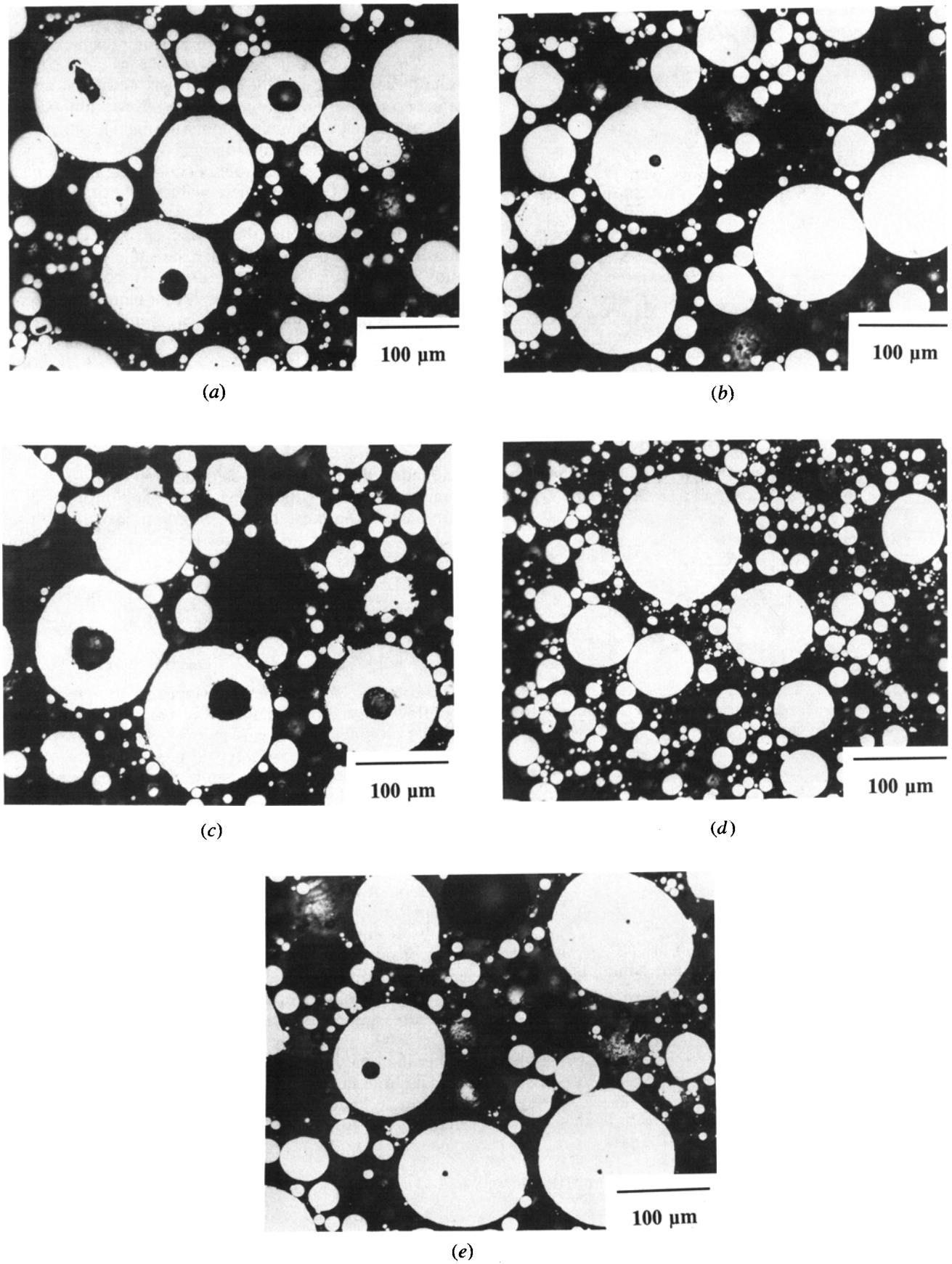

Fig. 2—Optical micrographs of the five as-atomized powders: (*a*) 304L Ar/Ar, (*b*) 304L Ar/N_2, (*c*) 304L N_2/Ar, (*d*) 304L N_2/N_2, and (*e*) 304L + Cr N_2/N_2.

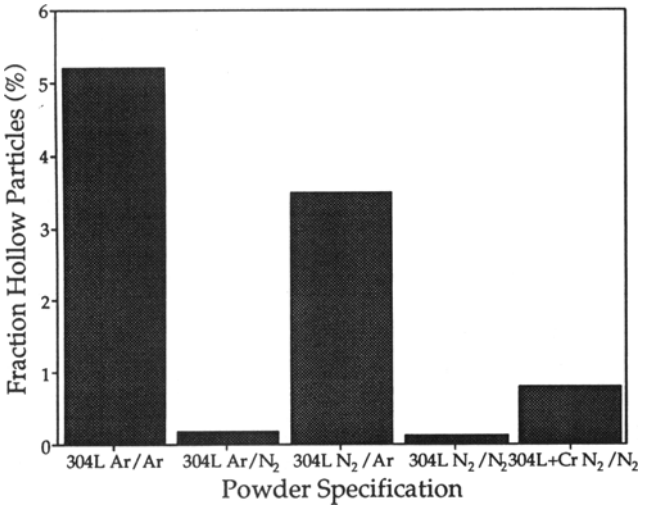

Fig. 3—Frequency of hollow particles observed in polished cross sections of the five powder types of this study.

content on the metal properties (such as surface energy and viscosity) do not significantly alter the gas/metal interactions. (This conclusion was also reached previously by VanStone *et al.*[10] for the nickel-base superalloy RENÉ 95 using a different atomizer design.)

*RENÉ is a trademark of General Electric Company, Fairfield, CT.

Therefore, it can be concluded that the changes in hollow particle frequency as a function of atomizing gas are not caused by physical effects upon the atomization process but rather a difference in the chemical behavior of the gas/metal system. It is proposed that differences in the hollow sphere frequency for the N_2- *vs* Ar-atomized powders are a direct effect of gas solubility and, possibly, diffusivity, since a low solubility for a species typically leads to a low diffusion coefficient. The solubility of nitrogen in Fe-18 wt pct Cr-8 wt pct Ni at 1700 °C and atmospheric pressure (the melt conditions) is 0.18 wt pct and continuously increases with decreasing temperature, even through the liquidus and solidus.[12] This behavior is in contrast to the generally low solubility of inert gases, including Ar, in liquid and solid metals. Therefore, any nitrogen gas which is entrapped in the molten metal would tend to dissolve and redistribute throughout the material, whereas entrapped argon remains as a gas-containing bubble.

The importance of gas solubility in pore formation is supported by additional experiments using N_2 or Ar as the atomizing gas for copper and RENÉ 95.[13] Neither gas has measurable solubility in Cu,[14,15] and powders atomized with these gases contained a large fraction of hollow particles (Ar atomized: 1.5 pct; N_2 atomized: 9.1 pct). Micrographs of the two copper powders are shown in Figure 8. In contrast, atomizing RENÉ 95 with N_2 rather than Ar virtually eliminated the occurrence of hollow powder particles, as shown in Figure 9. The solubility limit of nitrogen in RENÉ 95 is not known, but it has previously been shown to dissolve 0.043 wt pct nitrogen.[16] Thus, it appears that atomizing with a gas that has even slight solubility reduces and, in some cases,

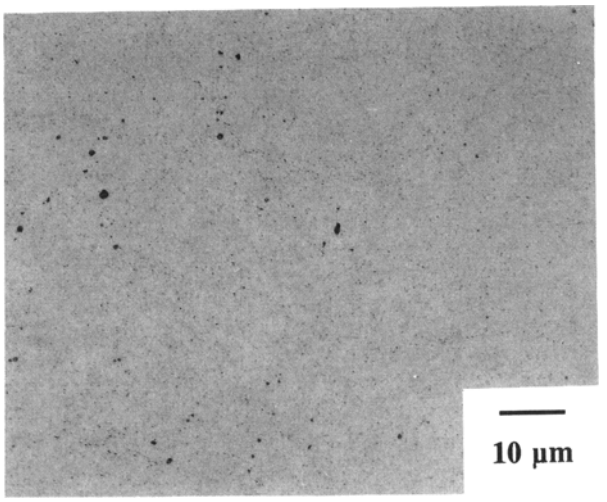

(*a*)

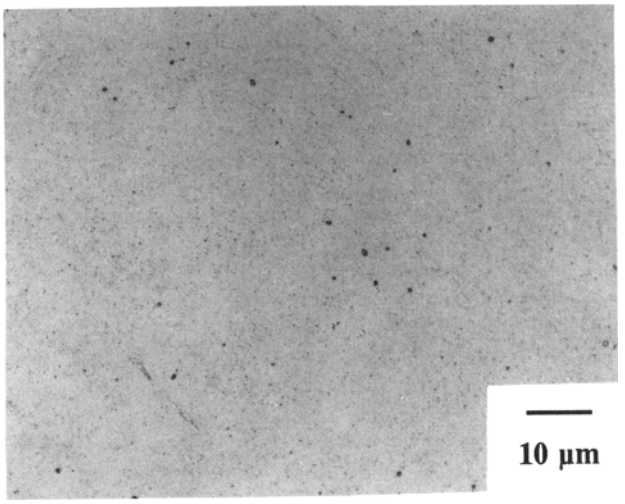

(*b*)

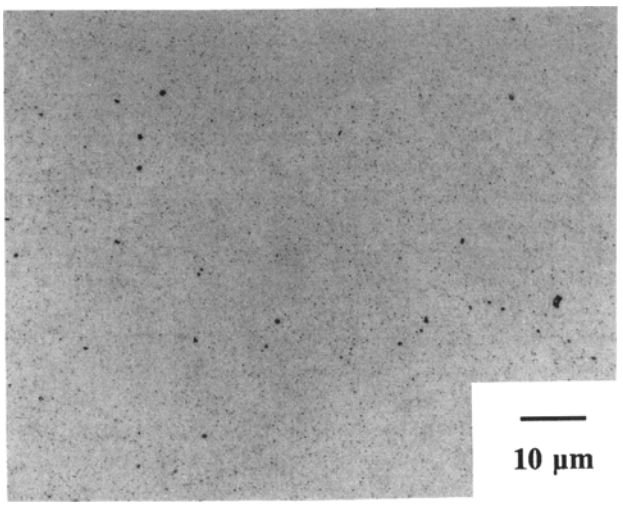

(*c*)

Fig. 4—Optical micrographs of (*a*) 304L Ar/Ar, (*b*) 304L N_2/N_2, and (*c*) 304L + Cr N_2/N_2 after hipping consolidation. In general, these materials have few voids and few inclusions over 1 μm in size.

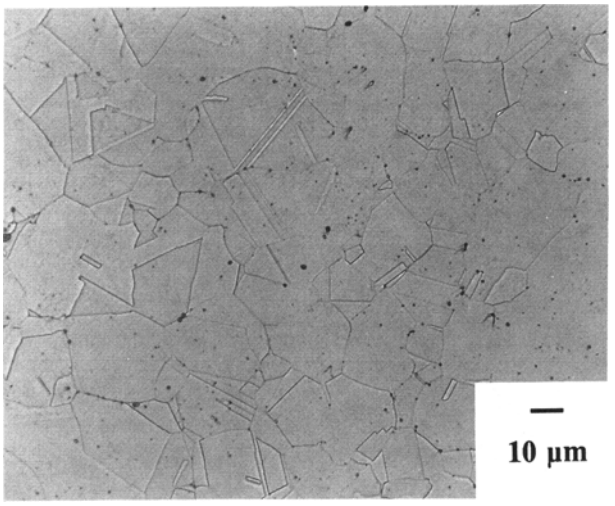

(*a*)

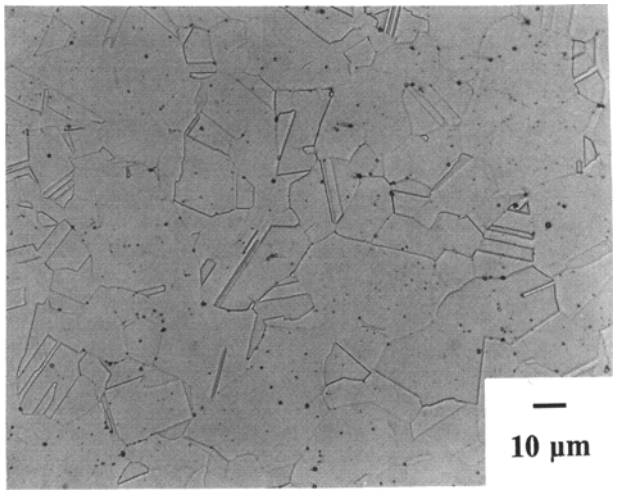

(*b*)

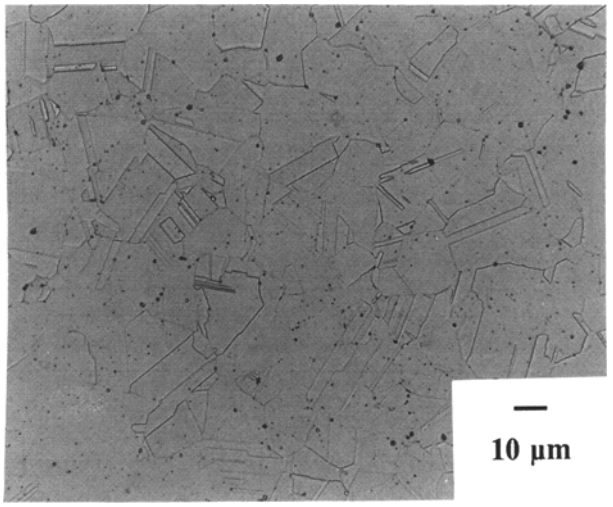

(*c*)

Fig. 5—Optical micrographs of the consolidated microstructure after etching: (*a*) 304L Ar/Ar, (*b*) 304L N_2/N_2, and (*c*) 304L + Cr N_2/N_2. Grain boundaries and twins are visible.

Table II. Nitrogen Content of the Specimens of this Study (Weight Percentages)

Base Alloy	Backfill Gas	Atomizing Gas	Nitrogen Content
304L	Ar	Ar	0.025
304L	N_2	Ar	0.157
304L	Ar	N_2	0.077
304L	N_2	N_2	0.148
304L + Cr	N_2	N_2	0.206

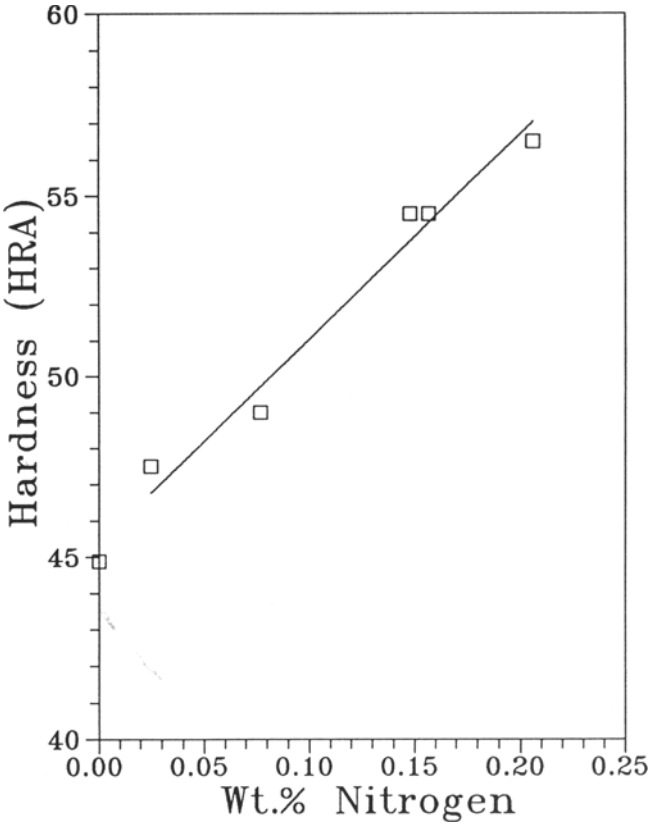

Fig. 6—Rockwell A hardness as a function of nitrogen content for the PM stainless steel alloys of this study.

virtually eliminates the occurence of hollow powder particles.

The elimination of hollow powder particles by utilizing nitrogen as the atomizing gas is technologically important, since the pores in inert gas atomized powders contain entrapped gas which is not removed by traditional consolidation methods. This entrapped gas will be compressed during high-temperature, high pressure processing (such as HIPping) and may be compressed to the extent that the consolidated material appears to be fully dense. However, this pressurized gas will cause pore reopening after high-temperature exposure without external pressure. This phenomena is illustrated in Figure 10, where micrographs of 304L Ar/Ar, 304L N_2/N_2, and 304L + Cr N_2/N_2 are shown after the consolidated materials were heat-treated at 1200 °C for 4 hours *in vacuo*. The compressed gas contained in the specimen produced with Ar-atomized powder (Figure 10a) resulted in many

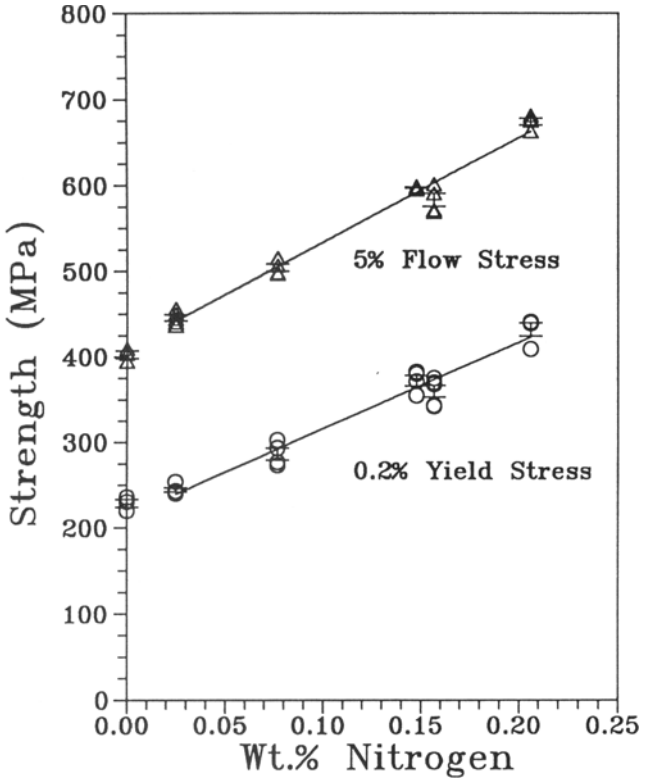

Fig. 7 — Yield strength and 5 pct flow stress as a function of nitrogen content.

large, angular pores, in addition to some fine pores. The N_2/N_2 specimens (both 304L and 304L + Cr) had only fine porosity. The cause of the fine porosity was not ascertained, but it is possibly due to small amounts of other entrained gases. The presence of the large, angular voids would be expected to reduce the fatigue resistance, ductility, and toughness of a final product produced with the Ar-atomized powders, since they act as stress concentrations. It should also be noted that the larger fraction of porous particles observed for the 304L + Cr N_2/N_2 powder (relative to 304L N_2/N_2) is not reflected in any pore reopening of the consolidated material after the 1200 °C heat treatment. This observation indicates that the nitrogen contained in the hollow powder particles of 304L + Cr N_2/N_2 is absorbed during consolidation, as would be expected from the increased nitrogen solubility at lower temperatures.

The fundamental mechanisms of liquid droplet formation during gas atomization are a topic of continuing interest. Previous work at NIST using high speed cinematography (20,000 images/s at 10^{-5} seconds exposure time) of the atomization plume has shown an extremely turbulent disruption sequence where large primary droplets are formed from sheets and ligaments. These primary droplets are drawn into the rapidly expanding supersonic gas flow and accelerated to velocities that exceed the speed-resolving limits of the camera (10 m/s for a 100 μm droplet).[6] This experimental limitation has prevented the mechanisms of fine droplet formation from being directly observed and, therefore, has inhibited the understanding of the formation of hollow powder particles in SIGMA. However, several theories have been

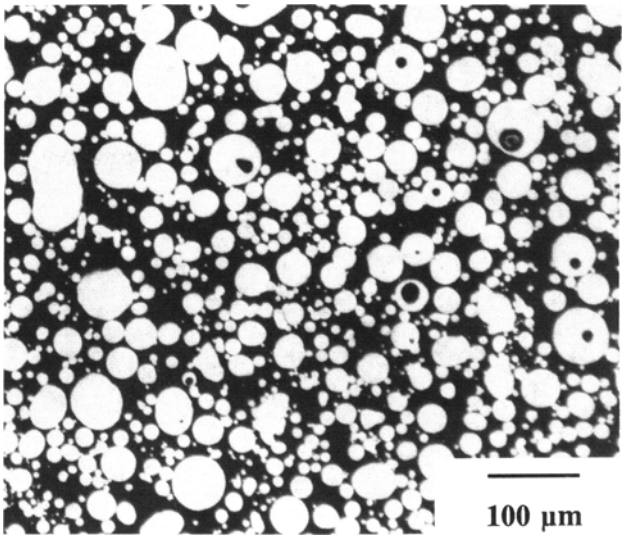

(*a*)

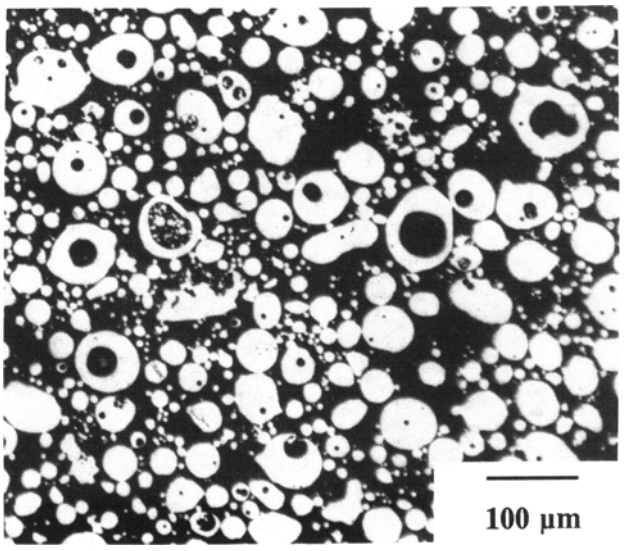

(*b*)

Fig. 8 — Optical micrographs of high purity copper powders atomized with (*a*) argon and (*b*) nitrogen.

previously introduced by other researchers to explain the origin of hollow particles during gas atomization.

(1) "Bag formation" is a mechanism where the liquid metal forms a closed sheet which contains gas. If the transport rate and/or solubility of the entrapped gas in the liquid is insufficient for it to escape or dissolve, the solidified powder particle will contain a bubble of the atomizing gas.[10,11,17]

(2) Solidification shrinkage is a mechanism where the center of the liquid droplet is the last metal to solidify, which leads to porosity due to the volume change associated with solidification. This hypothesis requires that the surface of the droplet solidify first, either by the presence of multiple nucleation sites or the rapid motion of surface dendrites.[10,18] The pores will not contain gas and, therefore, will not reopen on reheating.

(3) Reduction in gas solubility during solidification is a

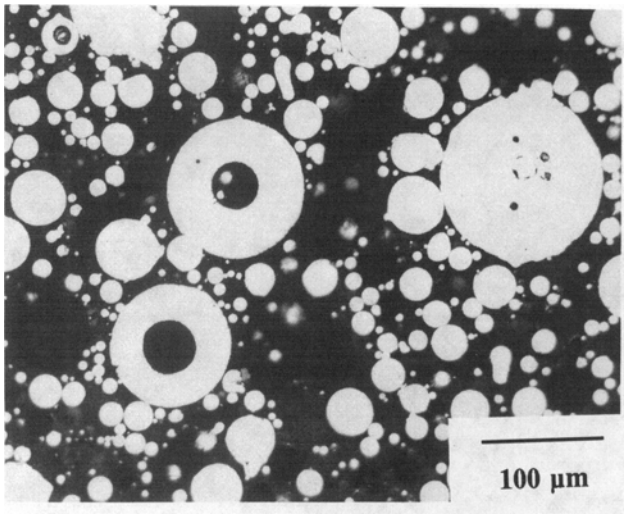

(*a*)

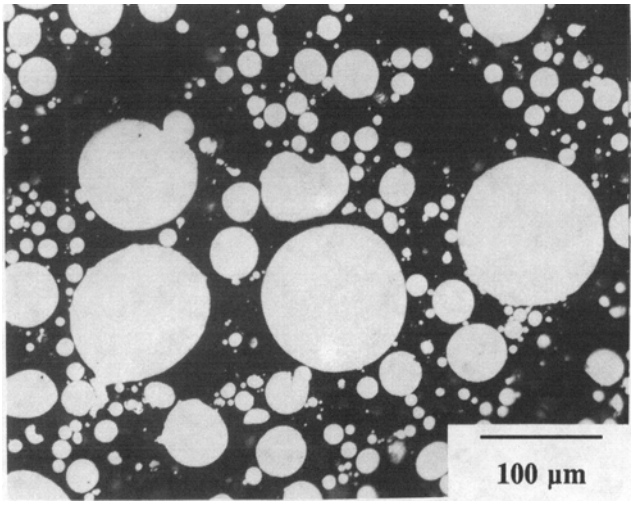

(*b*)

Fig. 9—Optical micrograph of RENÉ 95 powders atomized with (*a*) argon and (*b*) nitrogen.

mechanism where gas is evolved at the liquid/solid interface and is ultimately trapped inside the powder particle. An isolated volume of liquid is required as in mechanism (2) to form internal porosity.[10,11]

The results of this study indicate that solidification shrinkage is not a major cause of hollow particles in gas-atomized powders produced under these conditions using SIGMA. This conclusion is based on the reappearance of pores in the materials consolidated from the Ar-atomized powders after high-temperature, low pressure annealing, since shrinkage pores are not gas filled and would close during consolidation and would not reopen during heat treatment. It is not possible to establish which, if either, of the remaining mechanisms is dominant using only the results of the present study. However, atomizing with a soluble gas will reduce the amount of powder porosity caused by either mechanism (1) or (3). In the case of bag formation, the gas would be absorbed into the liquid metal during the atomization process.

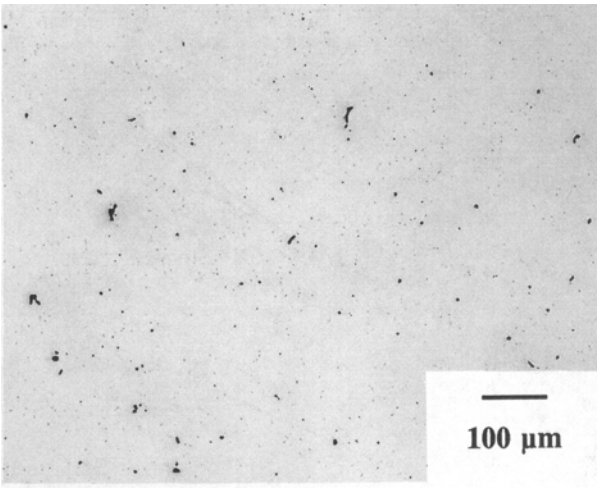

(*a*)

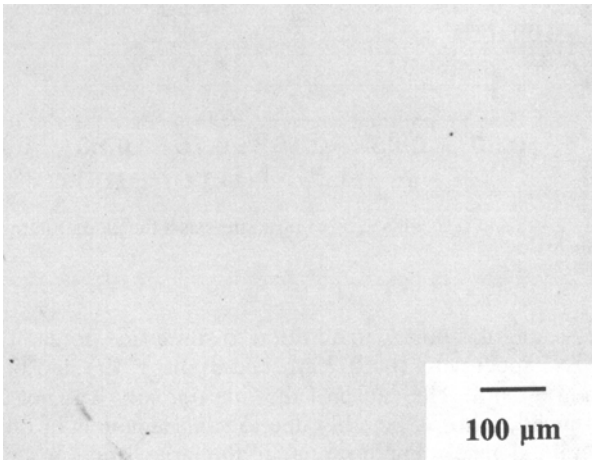

(*b*)

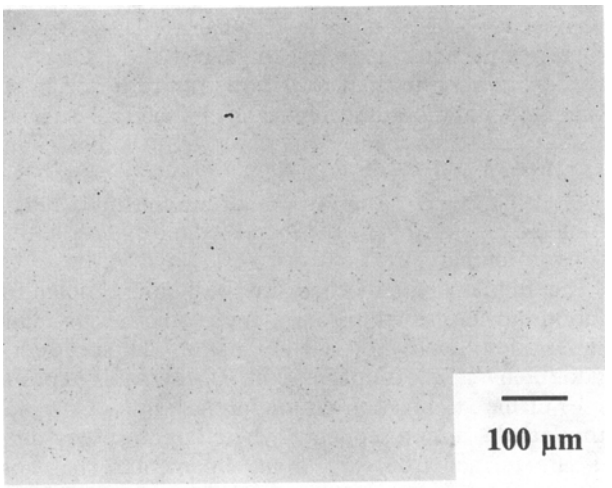

(*c*)

Fig. 10—Optical micrographs showing the changes in density of three of the alloys after heat-treating consolidated material *in vacuo* for 4 h at 1200 °C: (*a*) 304L Ar/Ar, (*b*) 304L N_2/N_2, and (*c*) 304L + Cr N_2/N_2. Note the numerous voids in the specimen made with Ar atomized powder and the lesser number of large voids in the other two materials.

Likewise, the gas bubbles would not form due to solubility effects, since the gas could remain in solution, particularly in the case of nitrogen and austenitic stainless steels where nitrogen solubility is greater at low temperatures. However, strong evidence for the occurrence of bag formation as an active droplet disintegration mechanism is shown in Figure 11, where a large number of small particles are contained within a single 150 μm powder particle. No other mechanism can result in the engulfment of other powder particles.

The quantitative porosity data of this study also indicate that some of the porosity found in Ar-atomized stainless steel powders is due to changes in gas solubility during solidification. This effect is clearly shown by considering the reduction in the fraction of hollow powder particles when the melt backfill is changed from Ar to N_2: 5.2 to 3.5 pct (Ar-atomized) and 0.76 to 0.13 pct (N_2-atomized). However, the effect of using Ar as a backfill gas is secondary compared to the primary effect(s) of using nitrogen as an atomizing gas, as discussed above.

B. *Nitrogen Content*

The nitrogen content of the powders was largely controlled by the melt chamber backfill gas and approached the equilibrium solubility at the melt temperature. However, the atomizing gas had an effect when the metal was melted under Ar and, therefore, unsaturated with nitrogen. These results indicate that (1) the molten stainless steel has sufficient residence time and mixing in the melt chamber to become saturated with nitrogen and (2) some nitrogen can be dissolved during the atomization of an unsaturated melt. The latter result is somewhat surprising, since gas atomization of particles in this size range is generally considered a rapid solidification process. However, it should be emphasized that nitrogen retention in austenitic stainless steels does not depend on one of the well-known benefits of rapid solidification, extended solubility, since nitrogen is increasingly soluble at lower temperatures.

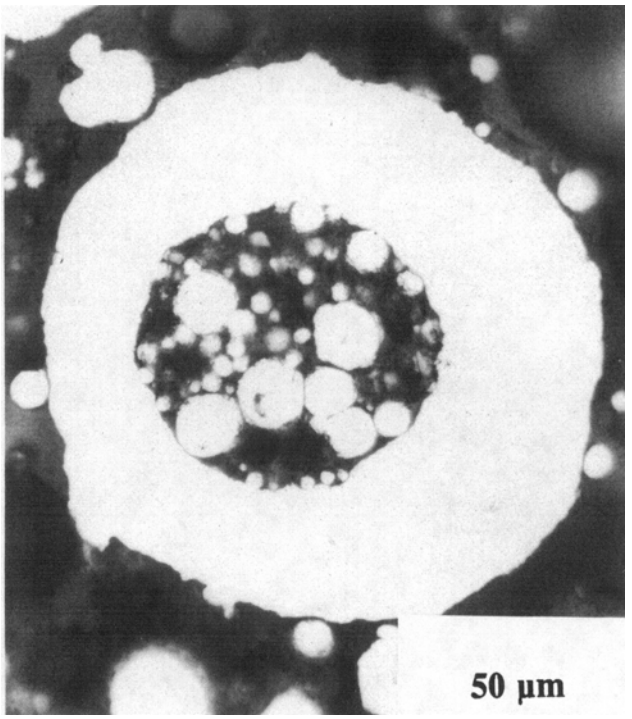

Fig. 11—Micrograph exhibiting bag formation during droplet disintegration in 304L stainless steel. Multiple fine powder particles are completely contained within a 150 μm powder particle.

The role of alloy content on nitrogen solubility was demonstrated in this study by changing the Cr content from 18 to 23 wt pct, with a concomitant increase in nitrogen concentration from 0.158 to 0.206 wt pct when backfilled and atomized with nitrogen. This result is consistent with previous studies of alloying effects on the nitrogen content of stainless steels [*e.g.*, References 13, 19, and 20], specifically that high nitrogen levels are favored by large chromium additions. The data of these other studies also suggest several other alloy modifications to further enhance nitrogen content: (1) decrease Ni levels; (2) add Mn as an alternative austenite stabilizer to Ni; and (3) add other strong nitride-forming elements, such as V, Nb, Ti, and Mo. While these ideas have not been applied to high nitrogen stainless steels produced by nitrogen melting and gas atomizing, the success of varying Cr levels indicates that the other composition modifications would also be beneficial.

C. *Mechanical Properties*

The limited mechanical property measurements of this study indicate that high nitrogen stainless steels processed in this manner are equivalent to similar alloys produced by other methods. Indeed, the increase in yield strength found in this study (1016 MPa/wt pct N) is significantly higher than the data compiled by Reed,[2] which showed values in the range of 310 to 710 MPa/wt pct N at room temperature. Several possible sources of this anomalously high strengthening increment can be found in the literature. The first such possibility is the presence of nanosized voids or cavities, reduced grain size, and high residual dislocation density.[21] The second possibility that has been considered is an increase in undercooling (and, therefore, a more refined microstructure) when N_2 is used as the atomizing gas.[10] Detailed microstructural characterization is necessary to determine if either of these proposed mechanisms is the cause of the additional increment of strengthening in austenitic stainless steels processed in this manner. Additional mechanical property measurements (tensile, impact, and fracture toughness testing) are planned. However, similar property enhancements, such as improved toughness, fatigue resistance, and creep resistance, are expected in materials processed using the methods discussed here as have been observed in high nitrogen austenitic stainless steels manufactured by other methods.

V. SUMMARY

It was demonstrated that high nitrogen austenitic stainless steel alloys can be processed by using nitrogen gas to backfill the melt chamber and to atomize. The nitrogen content of the alloys was most strongly effected by

the backfill gas, and the fraction of hollow powder particles was most strongly influenced by the atomizing gas. The latter result was interpreted in terms of the solubility of the atomizing gas in the liquid and solid metal, which was shown to also be true for gas atomization of copper and RENÉ 95. The nitrogen concentration was determined by the amount of nitrogen which dissolves in the liquid metal; higher chromium levels were shown to maximize the nitrogen content. The Ar-melted metal was able to dissolve some nitrogen when atomized with nitrogen. Hardness, compressive yield strength, and flow stress are substantially improved and are linearly dependent on the nitrogen content.

ACKNOWLEDGMENTS

The authors wish to thank R.J. Schaefer, R.D. Jiggetts, R.J. Fields, P.A. Boyer, and R.L. Parke of NIST and J.C. Rawers of the Bureau of Mines for their invaluable assistance in various aspects of this study. The financial support of GMJ by a National Research Council/National Institute of Standards and Technology Postdoctoral Associateship is gratefully acknowledged.

REFERENCES

1. A. Kendel, J.E. Truman, and K.B. Lomax: in *Proc. Int. Conf. High Nitrogen Steels*, J. Foct and A. Hendry, eds., The Institute of Metals, London, 1989, pp. 405-13.
2. R.P. Reed: *J. Met.*, 1989, Vol. 41 (3), pp. 16-21.
3. J. Rawers, J. Dunning, A. Petty, and R. Reed: *Adv. Mater. Proc.*, 1990, vol. 138 (2), pp. 50-52.
4. J. Rawers and L.J. Rawers: *J. Mater. Sci. Lett.*, 1991, vol. 10 (18), pp. 1101-02.
5. G. Stein, J. Menzel, and H. Dorr: in *Proc. Int. Conf. High Nitrogen Steels*, J. Foct and A. Hendry, eds., The Institute of Metals, London, 1989, pp. 32-38.
6. S.D. Ridder, P.I. Espina, and F.S. Biancaniello: in *Physical Chemistry of Powder Metals Production and Processing*, W. Murray Small, ed., TMS, Warrendale, PA, 1989, pp. 163-73.
7. P.I. Espina, S.D. Ridder, F.S. Biancaniello, and G.E. Mattingly: in *Characterization & Diagnostics of Ceramics & Metal Particulate Processing*, E.J. Lavernia, H. Henein, and I. Anderson, eds., TMS, Warrendale, PA, 1989, pp. 49-62.
8. F.S. Biancaniello, J.J. Conway, P.I. Espina, G.E. Mattingly, and S.D. Ridder: *Mater. Sci. Eng.*, 1990, vol. A124, pp. 9-14.
9. L. L'Estrade, H. Hallén, and R. Ljunggren: *Modern Developments in Powder Metallurgy*, MPIF, Princeton, NJ, 1988, vol. 20, pp. 187-203.
10. R.H. VanStone, F.J. Rizzo, and J.F. Radavich: in *Proc. 2nd Int. Conf. on Rapid Solidification Processing, Principles and Applications*, Reston, VA, March 23–26, 1980, R. Mehrabian, B.H. Kear, and M. Cohen, eds., Claitor's Publishing Division, Baton Rouge, LA, 1980, pp. 260-72.
11. B.H. Rabin, G.R. Smolik, and G.E. Korth: *Mater. Sci. Eng.*, 1990, vol. A124, pp. 1-7.
12. M. Kikuchi, M. Kajihara, and K. Frisk: in *Proc. Int. Conf. High Nitrogen Steels*, J. Foct and A. Hendry, eds., The Institute of Metals, London, 1989, pp. 63-74.
13. U.S. Patent No. 5,114,470, May 19, 1992.
14. B.B. Guliaev and G.F. Dvoretshaja: in *Phase Diagrams of Metallic Systems*, E.M. Savitskii, ed., Akad. Nauk SSSR, Moscow, 1968, pp. 267-73 (in Russian).
15. A.E. Vol: *Handbook of Binary Metallic Systems, Vol. 1*, U.S. Department of Commerce, Washington, D.C., 1966, p. 551.
16. U.S. Patent No. 4,140,528, February 20, 1979.
17. M. Pilch and C.A. Erdman: *Int. J. Multiphase Flow*, 1987, vol. 13, pp. 741-57.
18. G.H. Gessinger: *Powder Metallurgy of Superalloys*, Butterworth's, London, 1984, pp. 36-43.
19. W.M. Small and R.D. Pehlke: *Trans. AIME*, 1968, vol. 242, pp. 2501-05.
20. J.H. Feichtiger, A. Satir-Kolorz, and Zhang Xiao-Hong: in *Proc. Int. Conf. High Nitrogen Steels*, J. Foct and A. Hendry, eds., The Institute of Metals, London, 1989, pp. 75-80.
21. John E. Flinn, Jung Chan Bae, Thomas F. Kelly, and Gary E. Korth: *Metall. Trans. A*, 1992, vol. 23A, pp. 2557-65.